# Electrospinning of PCL Nanofibres - An Experimental and Numerical Study

**V Mamtha [1]\*, K K Janeesh[1], M P Sham Aan[2], C S Puneet[1]**

*[1]Department of Mechanical Engineering, RV College of Engineering, Bengaluru– 560 059*
*[2]Department of Chemistry, RV College of Engineering, Bengaluru-560 059*

## Abstract

Although electrospinning of PCL nanofibres is widely reported, studies including their surface roughness, porosity, pore radius and thickness are scarce. Numerical study on influence of length of needle, applied voltage and stand-off distance on electric field intensity is scanty. This paper presents influence of voltage, flow rate and solution concentration on formation of bead free PCL nanofibres and simulation of electric field intensity. Number of beads, diameter of nanofibres and porosity were obtained by SEM and Image J. Voltage 16 kV, flow rate 2 ml/hr and solution concentration 10 wt. % yielded nanofibres with nearly no beads. Their porosity, pore radius and surface roughness were 67.76 %, 0.83 μm and 1.35 μm respectively. Finite element Analysis results of maximum electric field intensity corresponded to stand off distance15 cm, needle length 15 mm and voltage 18 kV. Nanofibres electrospun at this voltage were large in diameter with beads.

*Keywords: Electrospinning, Beads, Electric field intensity, Fibre diameter*

## 1.0 Introduction

Emergence of nanofibres has gained much importance in the past few decades due to their potential applications in medical, engineering, defence, and other fields. Nanofibres are produced using methods such as melt spinning, force spinning, self-assembly, template synthesis and electrospinning. Electrospun nanofibres possess non-woven fibro porous structure, small pore size, large surface to volume ratio and good mechanical stability leading to widespread use in filtration, wound dressing, light weight garments, etc. In electrospinning, the flowing dielectric liquid, under the influence of applied electric field stretches from the needle to form a cone referred to as Taylor cone. Size of nanofibres depends on parameters such as solution concentration,

*\*Mail Address: V Mamtha, Assistant Professor, Mechanical Engineering Department, RV College of Engineering®, Bengaluru–59, Email: mamthav@rvce.edu.in, Ph: 99453 77144*

viscosity of polymer solution, applied electric field, stand-off distance and flow rate of polymer solution, temperature and humidity. Electric field being the main driving force has high influence on formation and morphology of nanofibres. Polymers such as Polyvinyl Acetate (PVA), Nylon 6, Poly methylene methacrylate (PMMA) and Polycaprolactone (PCL) are used for electrospinning. PCL has received attention in biomedical applications due to its biocompatibility and biodegradability and is suggested for wide range of applications. Electrospinning of PCL, its blends and composites has been attempted by many authors for tissue engineering scaffolds [1-5]. PCL can be electrospun with a number of solvents including, dichloromethane (DCM) [6-7] trifluoroethanol (TFE) [8] and hexafluoro-2-propanol (HFP) [9]. PCL and its blends are found satisfactory for electrospinning based on fibre dimension, properties and morphology. PCL is linear, resorbable, aliphatic polyester with properties such as nontoxicity, non-immunogenicity, solubility, low melting point (59°C to 64°C) and exceptional blend-compatibility.

Parametric study of electrospinning of PCL on fibre diameter. Electrospinning was conducted on polymer solutions (8 to 20 wt. %) PCL and 0.06 wt. % NaCl using 7:3 dichloromethane and methanol. Fibre diameter 300 nm and 1300 nm at 20 kV and 10 kV respectively with 8 wt. % PCL are reported [10]. Electrospinning on polyphenyl sulphone blended with Polyethylene glycol (PEG) using N-methyl-2-pyrrolidone and dimethylformamide was conducted. Up to 10 wt. % PEG and polyphenylsulphone 22 wt. % at 12 kV and stand-off distance18.75 cm were used [11].

Fibre dia 633 nm and porosity 72 % were obtained in 10 wt % PEG / PPS. Fibre dia. increased and porosity decreased with PEG addition. Reneker et al [12] reported electrospinning of 15 wt. % PCL dissolved in acetone. The authors reported new phenomenon of formation of columnar network called garland. At 7.5 kV and stand-off distance14 cm, fibre diameter was 5 mm. Md. Mahabub Hasan et al [13] developed tissue engineering scaffolds of electrospun PCL nanofibres of diameter 200 nm to 300 nm obtained at 20 kV, 15 cm stand-off distance and 10 % PCL/TFE. The authors reported sterilization of scaffolds using ethanol with no change in nanofibre morphology.

Artur et al [14] studied physical and mass transfer properties of simple PCL nanofibres and PCL nanofibres with encapsulated trypsin (E-PCL nanofibres). PCL nanofibres were highly hydrophobic and E-PCL nanofibres showed higher mechanical properties. Reduction in average pore size in E-PCL nanofibres was 30 % to 40%. Sherif Soliman et al

[15] investigated a method of modulating porosity in PCL scaffolds by tuning fibre diameter and fibre packing density. Scaffolds were classified as (a) microfibres with low fibre density (b) microfibres with high fibre density (c) nanofibres with low fibre density and (d) nanofibres with high fibre density. Liquid intrusion method was used to measure porosity of scaffolds. Larger pore size was obtained with larger fibre diameter. Lower fibre packing density resulted in higher pore size. Microfibres with low fibre density were found to have larger pore size (44 to 64 μm).

Somayeh Farhang Dehghan et al [16] optimized electrospinning parameters for polyacrylonitrile (PAN) nanofibres with MgO nanoparticles to obtain optimum fibre diameter and porosity of nanofibres for air filtration. Fibre diameter and porosity were computed using SEM. Minimum fibre dia was achieved with 9.6 wt. %, 15 kV and 12.5 cm stand-off distance. Porosity was directly related to fibre dia. Ning Wang et al [17] developed polyurethane (PU) based fibro-porous nanofibres to investigate effect of porous structure on permeability and fibre surface properties. Nanofibres of dia 347 nm, 738 nm and 1102 nm showed average pore size 800 nm, 870 nm and 1060 nm and pore volume of 44%, 63% and 68% respectively.

A few authors adopted finite element analysis for studying electric force and electric field distribution in electrospinning. Kang Weimin et al [18] studied the influence of distance between received plane and needle tube, radius of the received plane, size of needle tube and size of screen box for single needle and dual needle. Maximum electric field intensity (MEFI) and electrostatic force decreased rapidly with received distance between 100 mm and 200 mm and the same decreased slowly after received distance exceeded 200 mm. MEFI and electrostatic force increased nonlinearly with the radius of the received plane. Electrostatic force on needle tube increased, but MEFI decreased when the length of needle increased. With increase in size of screen box the electrostatic force increased nonlinearly. MEFI of single needle tube was $2 \sim 5 \times 10^6$ V/m and that of dual needle tubes was $1 \sim 3 \times 10^6$ V/m.

Duan Hong-wei et al [19] studied the electric field structure of plate-plate type electrospinning using ANSYS. Vector distribution of nozzle on spinneret pipe was obtained. Maximum field strength of $0.49 \times 10^6$ V/m appeared at the position of spinning pipe orifice. Electric field strength decreased with increase in the surface area and tip to collector distance. 20 wt.% concentration, 15 kV applied voltage, 150 rpm drum speed were used to electrospin Polyacrylic acid (PAA). Nanofibres of diameter 675 nm, 500 nm and 400 nm corresponded to the spinning distances 16 cm,

20 cm and 24 cm. Similarly, 520 nm, 795 nm and 1025 nm for the flow rates 0.5 ml/hr, 1 ml/hr and 1.5 ml/hr. Hadi Samadian et al [20] modelled electric field and investigated effect of solution concentration and applied voltage on electrospinning of polyacrylonitrile. Electric field p at the nozzle and electrospinning zone was predicted by Finite Element Analysis. Contour of the electric field was concentrated at the needle tip and reduced rapidly towards surface of the collector. Increase in solution concentration of polymer from 7 wt. % to 11 wt. % led to increase in the diameter of nanofibres from $77.76 \pm 19.44$ nm to $202.42 \pm 36.85$ nm. Increase in applied voltage from 15 to 25 kV resulted in change in mean diameter of nanofibres from $60.96 \pm 25.11$ nm to $79.91 \pm 29.94$ nm.

Jin-gang Jiang et al [21] analysed electric field structure of a needle-plate type electrospinning device using ANSYS. Electrospun PVDF/PEI composite films were fabricated using varied solvent ratios of N, N-dimethylformamide and tetrahydrofuran. Peak electric field intensity was $2.64 \times 10^6$ V/m. XRD showed that under the influence of an electric field force the crystal form transformed from α into β and δ. With increase in tetrahydrofuran, fracture elongation and fracture stress of PVDF/PEI initially increased and subsequently decreased.

Parametric study of electrospinning of PCL nanofibres is reported by several authors. However, characterization of nanofibres for thickness, porosity, mean pore radius, number of beads and surface roughness is scarce. Even though simulation of electrospinning for electric field intensity is reported, such studies including influence of length of needle, stand-off distance and voltage on the electric field intensity is scarce. The main objective of this research was to investigate the influence of voltage, flow rate and solution concentration on fibre diameter, thickness, porosity, mean pore radius, surface roughness and number of beads and to simulate electric field intensity as a function of length of needle, stand-off distance and voltage.

## 2.0 Experimental Details

### 2.1 Materials, Processes and Characterisation

*2.1.1 Materials*

Polycaprolactone (PCL) ($C_6H_{10}O_2$) n, Mw: 80,000 g/mol, Density: 1.145 g/cm$^3$ were obtained from Sigma Aldrich. N, N-dimethyl formamide (DMF) solvent 99% ($C_3H_7N$, Mw: 73.09g/mol), dichloromethane (DCM) 99% ($CH_2Cl_2$: Fisher scientific, Mw: 84.93 g /mol) and aluminium foil were used for the fabrication of PCL nanofibres.

## 2.1.2 Electrospinning of PCL nanofibres

Horizontal Electrospinning System with power supply up to 30 kV, programmable syringe pump, 10 ml syringe, 0.2 mm diameter stainless steel needle and grounded drum collector with variable speed up to 1000 rpm and set to rotate at 500 rpm were used for fabricating PCL nanofibres. Solvents (DCM : DMF in 1:1.5), solution concentration (8 to 12 wt %), flow rate (1 to 2 ml/hr), applied electric field (14 to 18 kV) and constant stand-off distance150 mm were used for the experimental study (Table 1). The nanofibres were dried at room temperature.

## 2.2.3 Study of electrospinning parameters for bead free nanofibres

Optimisation of electrospinning parameters such as solution concentration, flow rate and applied voltage is essential to achieve uniform and bead free nanofibres of least fibre diameter and required porosity. Flow rate and solution concentration were kept constant and applied voltage was varied. Voltage which resulted in least fibre diameter with no beads was identified based on SEM micrographs. Further experiments were conducted maintaining voltage and solution concentration constant and varying the flow rate. Based on SEM micrographs, the flow rate which corresponded to least fibre diameter with no beads was identified. In the next level, applied voltage and flow rate were maintained constant and solution concentration was varied for obtaining least fibre diameter with no beads. The sequence of experiments is presented in Table 1.

**Table 1.** Experimental parameters for electrospinning of PCL nanofibres

| Expt. No | Parameters | | |
|---|---|---|---|
| | Drum Speed: 500 rpm | | |
| | Tip to collector distance: 15 cm | | |
| | PCL, wt % | Flow Rate (ml/hr) | Applied Voltage (kV) |
| 1 | 10 | 1 | 10 |
| 2 | 10 | 1 | 12 |
| 3 | 10 | 1 | 14 |
| 4 | 10 | 1 | 16 |
| 5 | 10 | 1 | 18 |
| 6 | 10 | 1.5 | 16 |
| 7 | 10 | 2 | 16 |
| 8 | 8 | 2 | 16 |
| 9 | 12 | 2 | 16 |

### 2.2.4 Morphology of PCL nanofibres

The electrospun PCL nanofibres were gold sputter coated for 30 seconds for SEM (Zeiss Supra 35VP field emission SEM) studies. Diameter of nanofibres was measured by using ImageJ software based on ten measurements for each trial. Mean pore radius and number of beads were obtained using ImageJ software.

### 2.2.5 Thickness, porosity and pore radius of PCL nanofibres

Thickness of bare aluminium foil and the foil coated with PCL were measured using micrometer. Based on these, the thickness of electrospun nanofibres was computed. Three readings were taken for each sample. Apparent density of fibres was obtained using equation (1).

$$\rho = \frac{m}{A \times t} \qquad (1)$$

where 'm' is the mass, 'A' is area ($16 \ cm^2$) and 't' is thickness of nanofibres. Mass of the nanofibres was obtained based on the differential masses. Mean pore radius ($\bar{r}$) was obtained by ImageJ software. Porosity ($\epsilon$) of the nanofibres was computed using equation (2).

$$\epsilon = \frac{\rho_0 - \rho}{\rho_0} \times 100 \qquad (2)$$

$\rho$ is the apparent density of nanofibres and $\rho_0$ is average density of the PCL polymer ($1.145 \ g/cm^3$).

Mean pore radius ($\bar{r}$) was computed using equation (3)

$$\bar{r} = \frac{\sqrt{\pi}}{4} \left( \frac{\pi}{2 \log\left(\frac{1}{\epsilon}\right)} - 1 \right) d \qquad (3)$$

$\epsilon$ is the porosity and 'd' is mean fibre diameter obtained from the SEM image using ImageJ.

### 2.2.6 Surface roughness of nanofibres

Surface roughness of the nanofibrous membranes was measured using Surface roughness measuring SJ-210 [Measuring range- X axis: 17.5 mm, Z axis: (14200μin -7900μin~+6300μin) / 360μm (-200μm ~ +160μm)] and sampling length 0.08, 0.25, 0.8 and 2.5 mm)] consisting of a stylus with a diamond tip. Surface roughness of the nanofibrous membranes was measured in terms of Ra, Rq and Rz.

Average roughness (Ra) is computed using (4)

$$Ra = \sum_{n=1}^{N} \frac{|Zn-\overline{Z}|}{N} \ ---- (4)$$

where Zn is the height at sample point n, $\overline{Z}$ is the height of the center plane, and N is the total number of points in the sample area.

Root-mean-squared roughness (Rq) is given by the standard deviation of the Z values for the sample area and is computed using (5)

$$Rq = \sqrt{\sum_{n=1}^{N} \frac{|Zn-\overline{Z}|}{N}} ---- (5)$$

Rq contains squared terms and hence large deviations from the average height are weighted more heavily than for the mean roughness.

Maximum height of the profile (Rz) is frequently used to check whether the profile has protruding peaks that might affect static or sliding contact function.

*2.3 Results and Discussion*

*2.3.1 Nanofibre diameter*

SEM micrographs and distribution of fibre diameter for the parameter combinations of nine experiments of Table 1 are presented in Fig. 1. Mean fibre diameter for varied applied voltage, flow rate and solution concentration is shown in Table 2. Mean fibre diameter decreased with increase in voltage. At low voltage or low electric field strength, there is less stretching of the jet and hence larger fibre diameter. The jet originated from the Taylor cone leads to bead free spinning. With increase in voltage, the volume of the drop at the tip decreases, causing the Taylor cone to recede. The jet originates from the liquid surface within the tip leading to increase in number of beads. With further increase in voltage, the Taylor cone becomes invisible leading to increase in the number of beads [22]. In the present research with increase in voltage from 10 kV to 12 kV, the number of beads increased from 26 to 55. With change in voltage from 16 kV to 18 kV, the beads increased from 52 to 86.
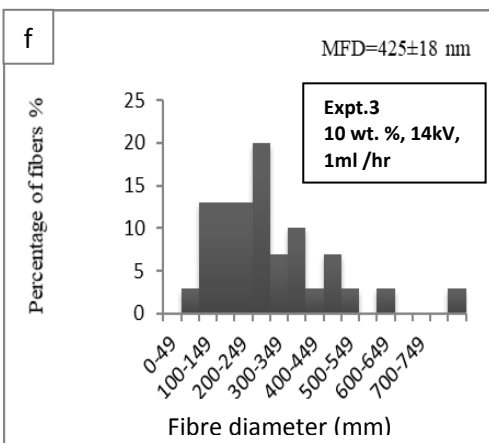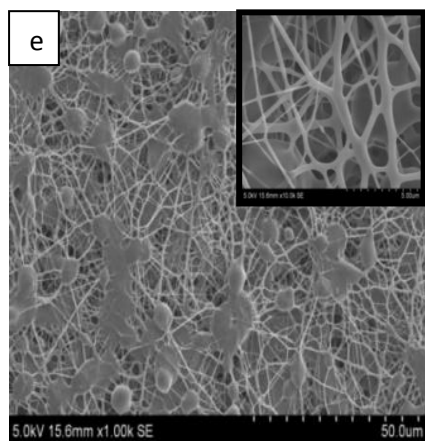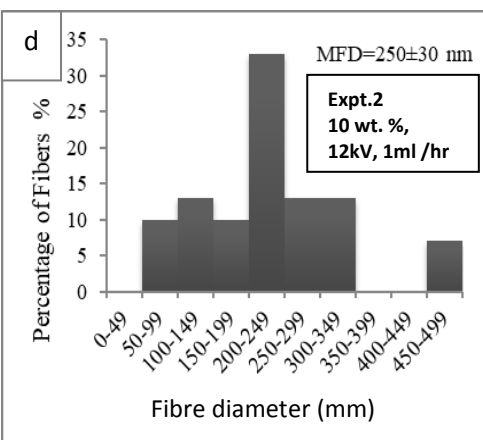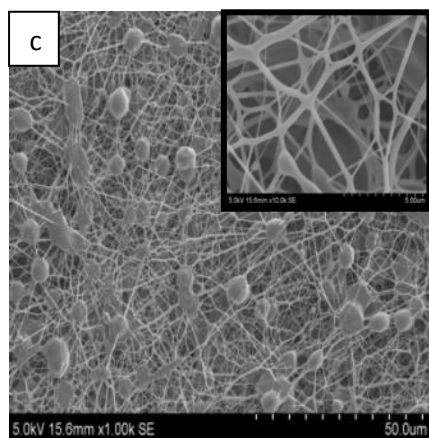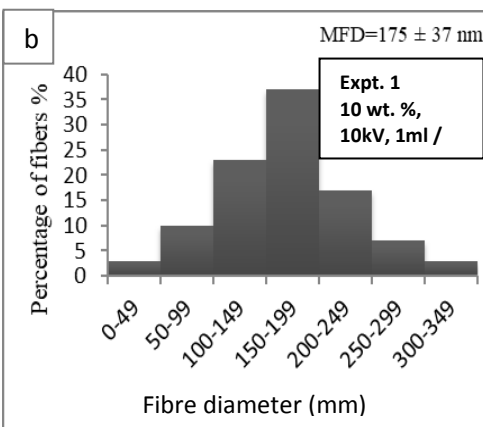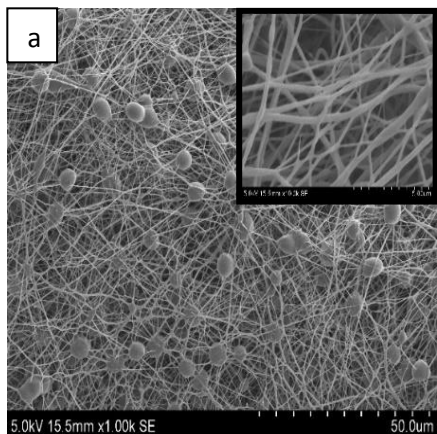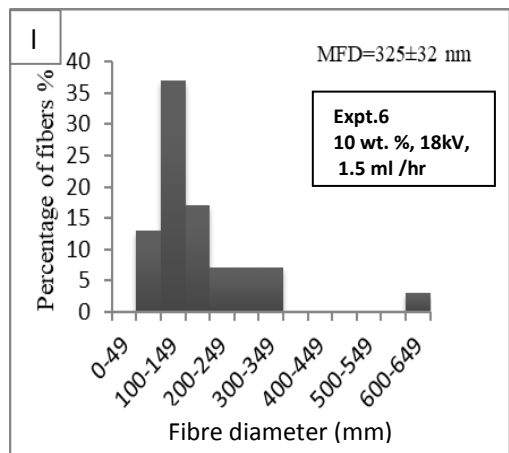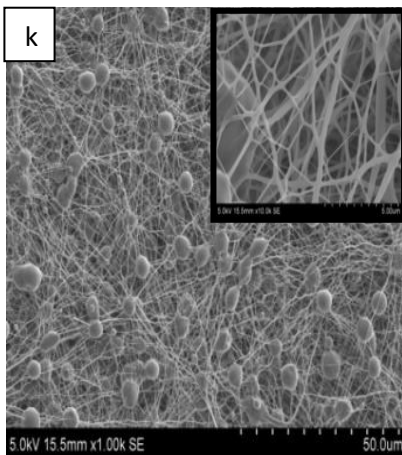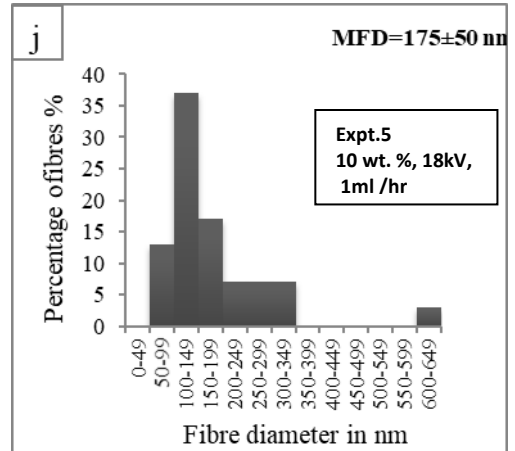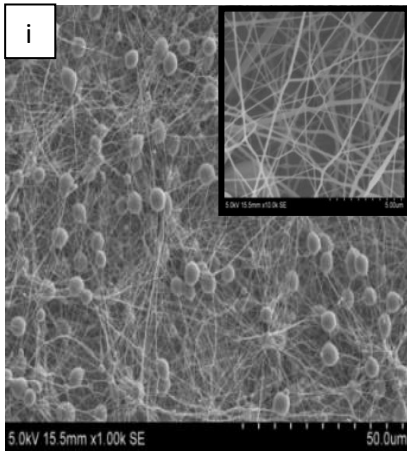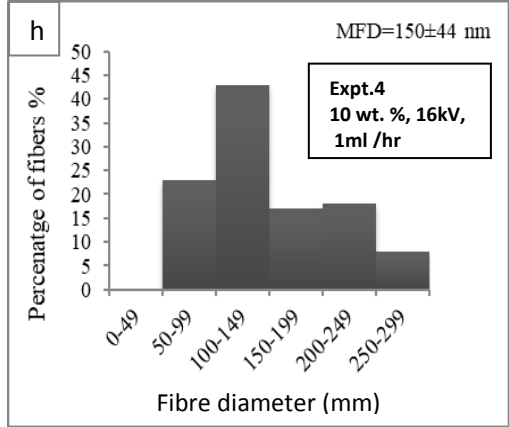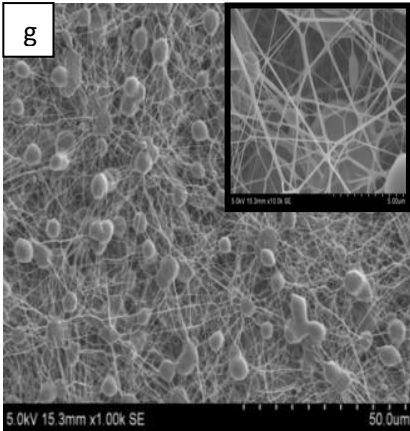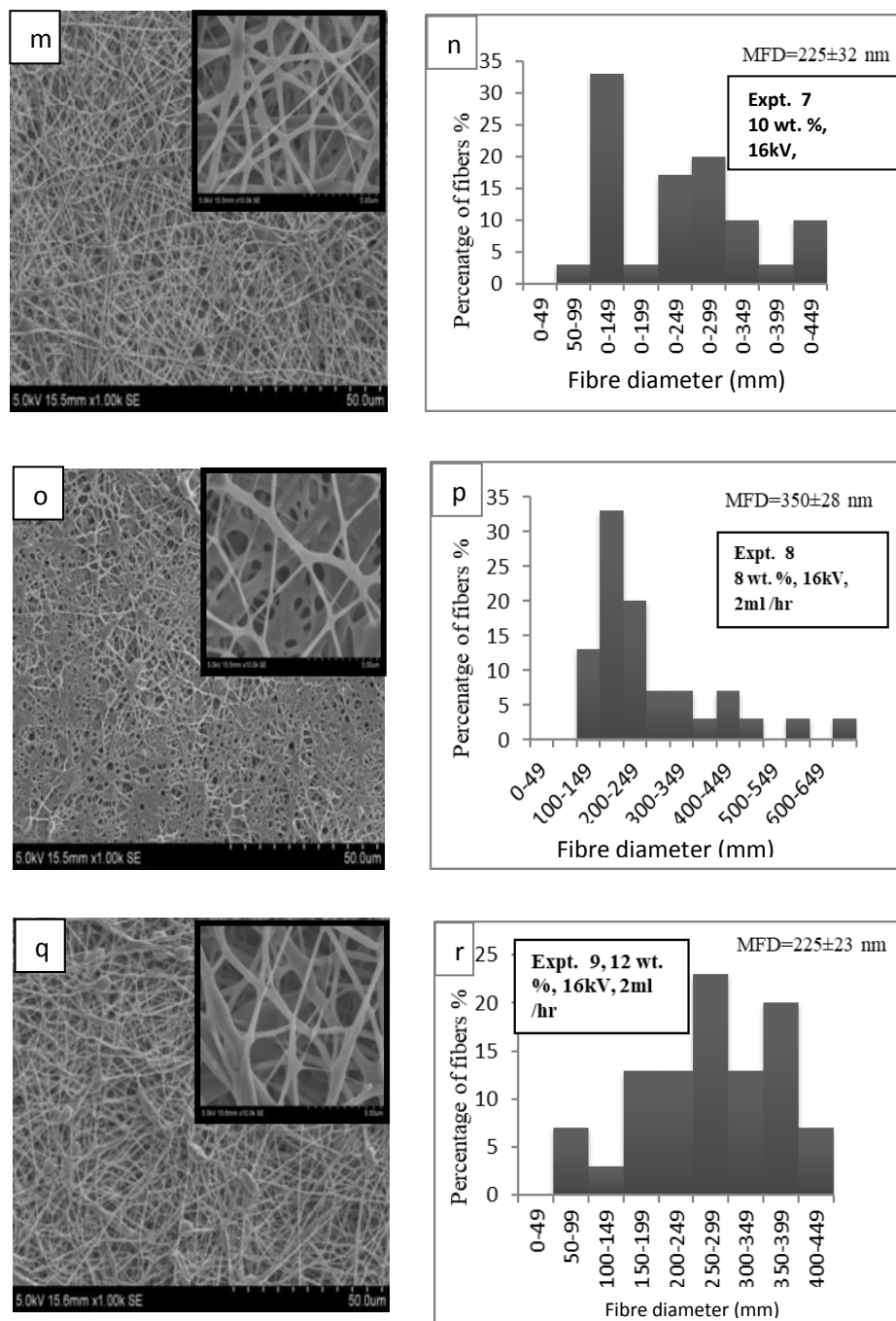
**Fig. 1.** SEM images and fibre dia. distribution of PCL nanofibres for parameter combinations of Expt. 1 to 9

Mean fibre diameter increased with increase in flow rate. At higher flow rate, quantity of solution delivered to the needle tip is higher which renders the jet to collect the solution quickly from the needle tip and it results in larger fibre diameter [23]. With increase in flow rate from 1 ml / hr to 2.0 ml / hr the fibre diameter increased from $175 \pm 50$ to $225 \pm 32$ nm with significant decrease in beads from 52 to 7. However, increasing the flow rate beyond a critical value not only leads to increase in pore size and fibre diameter but also to bead formation due to incomplete drying of the nanofibre jet during the flight between the needle tip and metallic collector.

Mean fibre diameter increased with solution concentration. Higher solution concentration increases the macromolecular chain entanglements and viscoelastic force. Number of beads increased from 4 to 10 with increase in solution concentration from 8 to 10 wt. %. Increase in concentration obstructs the solution through the tip of the needle leading to defective or beaded nanofibres. Beads were observed at 8 wt. % (7 beads) and 12 wt. % (10 beads) solution concentration. At 10 wt. % more uniform fibres with a few beads (4 beads) were obtained. In general, it can be concluded that the influence of applied voltage and flow rate on fibre diameter and number of beads was not as significant as that of solution concentration (Table 2). At 16 kV, 2 ml / hr and 10 wt. %, uniform fibres with least number of beads were obtained and hence this parametric combination was considered best.

**Table 2.** Parametric influence on fibre diameter and morphology of PCL nanofibres

| Effect of Applied Voltage | | | Effect of flow rate | | | Effect of Solution concentration | | |
|---|---|---|---|---|---|---|---|---|
| Voltage (kV) | Fibre dia. (nm) | Bead count | Flow rate (ml/hr) | Fibre dia. (nm) | Bead count | Solution Concentration | Fibre dia. (nm) | Bead count |
| 10 | 175±37 | 26 | 1 | 175±50 | 52 | 8 | 350±28 | 4 |
| 12 | 250±30 | 55 | 1.5 | 325±32 | 48 | 10 | 225±32 | 7 |
| 14 | 425±18 | 22 | 2 | 225±32 | 7 | 12 | 225±23 | 10 |
| 16 | 150±44 | 52 | | | | | | |
| 18 | 175±50 | 86 | | | | | | |

## 2.3.2 Thickness, porosity and pore radius of PCL nanofibres

Nanofibres were characterized for thickness, porosity and pore radius and the results are shown in Table 3.

**Table 3.** Thickness, porosity, and pore radius of PCL nanofibers

| Expt No. | Fibre Dia (nm) | Membrane Thickness (mm) | Porosity Nanofibres, % ($\epsilon$) | Mean pore radius ($\bar{r}$), μm | $\bar{r}$ ImageJ in μm |
|---|---|---|---|---|---|
| 1 | 175± | 0.017 | 71.30 | 0.70 | 0.74 |
| 2 | 250± | 0.023 | 67.44 | 0.84 | 0.89 |
| 3 | 425± | 0.037 | 69.52 | 1.19 | 1.06 |
| 4 | 150± | 0.015 | 47.33 | 0.23 | 0.34 |
| 5 | 175± | 0.012 | 84.54 | 1.03 | 1.19 |
| 6 | 325± | 0.016 | 81.57 | 1.28 | 1.25 |
| 7 | 225± | 0.018 | 67.76 | 0.83 | 0.80 |
| 8 | 350± | 0.007 | 51.47 | 0.50 | 0.57 |
| 9 | 225± | 0.017 | 70.46 | 1.11 | 1.20 |

Porosity of 67.76 % was observed for nanofibres fabricated at 16 kV, 2ml/h and 10 wt. %. The correlation between applied voltage and percent porosity was initially negative followed by positive relationship when flow rate and solution concentration were kept constant. A negative correlation existed between percent porosity and flow rate when keeping applied voltage and solution concentration constant in a way that increase in flow rate lead to decrease in porosity due to larger fibre diameters obtained. Positive relationship existed between solution concentration and percent porosity when applied voltage and flow rate were kept constant in a way that increase in concentration leads to increase in porosity [16].The difference in the mean pore radius obtained experimentally and that by ImageJ can be attributed to the small area considered and complexity involved in locating the pores in SEM.

### 2.3.3 Surface roughness of PCL nanofibres

Texture of a surface is measured by surface roughness. Membrane roughness is the nonconformity of the membrane topography from the ideal smooth surface. Interaction of a membrane surface with its environment is determined by the roughness of the membrane. For example, surface roughness is important in evaluating the performance of a membrane as it may influence the transmembrane transport and fouling potential of the membrane [24]. Surface roughness also determines the wettability of the membrane. Surface roughness and pore size distribution may also be correlated [25]. Surface roughness of PCL

nanofibrous membranes measured in terms of Ra, Rq and Rz are presented in Table 4. Lowest values of Ra (1.672 µm) and Rq (1.351µm) corresponded to fibre diameter 225 + 32 nm and pore radius 0.83 µm. Highest values of Ra and Rq corresponded to thinnest nanofibres i.e. 150 + 44, which is in agreement with [26]. Surface roughness and fibre diameter of nanofibres are inversely related. This is because thinner diameters provide higher specific surface areas of nanofibrous membrane and rugged surface of nanofibres. Hyung et al [27] reported that fibre diameter and surface roughness Ra of PCL mats are directly related because of alignment of fibre thickness as well as pore size on the surface of the mat.

**Table 4.** Surface roughness of PCL nanofibrous membrane

| Expt. No. | Fibre dia., nm, (Pore radius, µm) | Surface Roughness of PCL nanofibrous membrane | | |
|---|---|---|---|---|
| | | Ra (µm) | Rq (µm) | Rz (µm) |
| 1 | 175± 37, (0.70) | 3.21 | 3.89 | 15.50 |
| 2 | 250±30, (0.84) | 4.02 | 4.71 | 18.62 |
| 3 | 425±18, (1.19) | 2.44 | 3.06 | 13.06 |
| 4 | 150±44, (0.23) | 4.18 | 2.57 | 10.34 |
| 5 | 175±50, (1.03) | 2.09 | 2.52 | 9.91 |
| 6 | 325±32, (1.28) | 2.22 | 2.71 | 12.10 |
| 7 | 225±32, (0.83) | 1.35 | 1.67 | 7.94 |
| 8 | 350±38, (0.50) | 1.36 | 1.69 | 7.50 |
| 9 | 225±23, (1.11) | 1.72 | 2.17 | 10.56 |
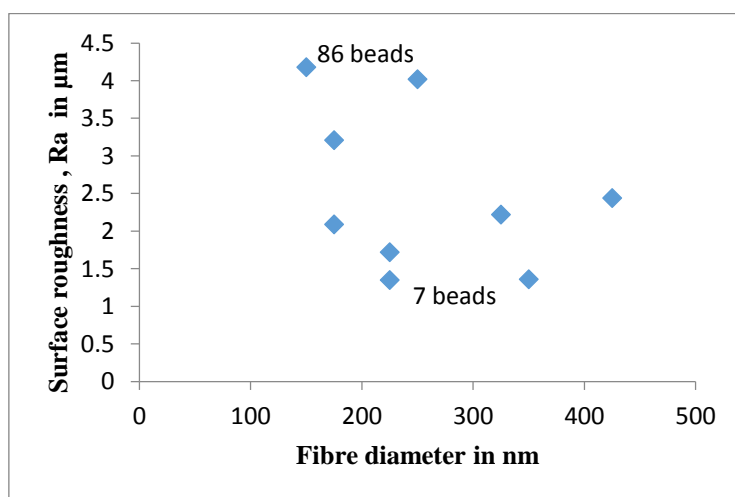


**Fig. 2.** Fibre diameter vs. surface roughness of PCL nanofibrous membrane

Beads are considered as defects as they provide additional stress points which can affect the membrane's mechanical properties. However, micro or nanobeads on the electrospun membranes can impart additional roughness to the membrane surface and hence enhance the membrane hydrophobicity, if properly designed.

Surface morphology of the nanofibrous membrane shows large amount of protrusions, hills and valleys, providing micro scale and nanoscale roughness that could possibly increase the hydrophobicity of the surface [28] .In the present work highest number of beads were observed for nanofibres at 10 wt. %, 16 kV and 1 ml/hr with a surface roughness of 4.18 μm and porosity of 47

# 3.0 Simulation of Electric field intensity using ANSYS HFSS

Electric field is the main driving force in electrospinning for the formation of nanofibres. Hence, thorough understanding of the distribution of electric field is vital for achieving quality nanofibres. Finite element simulation can guide parametric optimization in electrospinning. Finite element analysis was performed to study relationship between electric field intensity and system parameters, namely, applied voltage, length of the needle and stand-off distance. Solid works was used to create 3D model of the needle (3.8 mm inner dia. and 4.5 mm outer dia.) and drum collector (50 mm dia. and 200 mm long) of the electrospinning system. Analysis was performed to study the effect of needle length (15, 20, 25 and 30 cm), stand-off distance(10, 15, 20 and 25 cm) and applied voltage (10, 14, 16 and 18) on the electric field intensity. Electric field generated for different electrospinning parameters were analysed using ANSYS HFSS. Excitations were assigned to drum collector as 0 kV and needle as (10, 14, 16 and 18kV). Stainless steel for needle and aluminium for drum collector were defined and electric field intensity plots were generated as shown in Fig. 3 to 5

## 3.1 Results and Discussion

The electric field intensity vector distributes the electric field lines concentrated around the electrospinning nozzle. Electric field intensity is directed towards the collector. In the vicinity of the nozzle the electric field intensity is high and is critical for the formation of a stable jet.
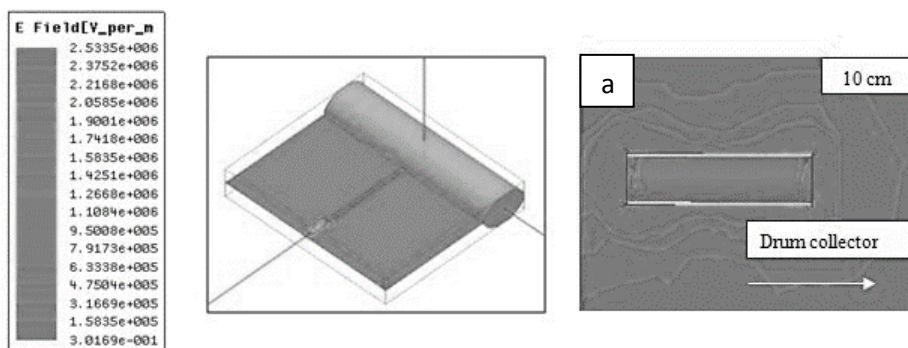
**Fig. 3.** Electric field intensity at varying Tip to Collector Distance

Fig 3. shows the electric field intensity with varying tip to collector distance. Maximum electric field strength of $3.96 \times 10^6$ was obtained at 15 cm. Electrostatic force on the spinning solution varied with increasing tip to collector distance. At lower stand-off distance, the solvents do not have enough time to evaporate, resulting in thicker fibres being deposited on the collector. Changing the stand-off distance affects the jet flight time and electric field strength. Larger distance offers more time for jet stretching and solvent evaporation before depositing on the collector. This results in decrease in fibre diameter. Also, spinning distance is inversely proportional to the electric field strength that result in less stretching forces which leads to formation of fibres with larger diameter. Final fibre diameter is determined by the balance between the two effects. [23]. In the present work stand-off distance was maintained constant at 15 cm which is consistent with the simulation results.
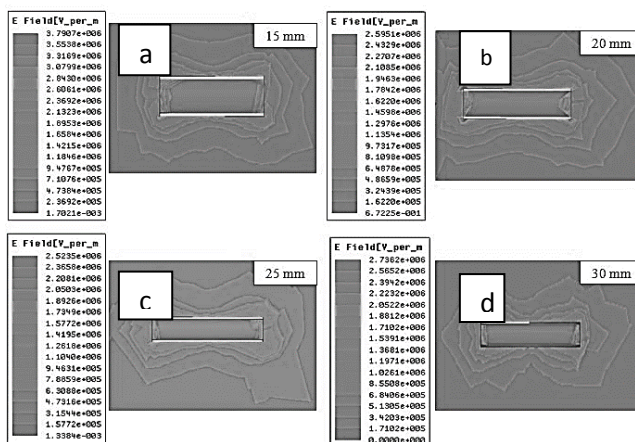


**Fig. 4.** Electric field intensity at varying length of needle

Fig. 4 shows the electric field intensity with varying length of the needle from 15 mm to 30 mm, the electric field intensity increased to a maximum value of $3.79 \times 10^6$ V/m and then decreased with the increase in length of the needle. Length of needle will affect the degree of macromolecule orientation of nanofibres. Larger length of the needle leads to longer time for macromolecule array and the macromolecules have higher degree of orientation resulting in improved mechanical properties of nanofibres. Electrostatic force on the needle and hence on the spinning solution decreases nonlinearly with increase in length of needle which does not favour the formation of Taylor cone and thinning of fibres [18]. Hence shorter length of the needle is preferred. Increase in needle length, the macromolecules are more and more orderly in the moving jet, so the friction among molecule chains is smaller and smaller. The tensile stress decreased with the increase of needle length. When the order of macromolecules reached the limit, the tensile stress tends to stable [29].

Fig. 5 shows the electric field intensity with varying applied voltage from 10 kV to 18 kV. It was observed that the electric filed intensity increased with the applied voltage. Maximum electric field intensity obtained was $4.21 \times 10^6$ V/m at 22 kV. At low applied voltage, the strength of the electric field is low which results in less stretching of the jets before they are deposited on the collector. At higher voltage, more solution is drawn from the solution droplets, which favours the formation of thicker fibres due to thicker initial jets. When the applied voltage exceeds a certain limit, jet elongation becomes the dominant factor. At this stage, electric field strength is high resulting in strong stretching of the jets. In the present work bead free nanofibres were obtained at 16 kV which is inconsistent with the simulation results. Although higher applied voltage results in high electric field intensity, the nanofibres generated would be thicker with beads. Since nanofibres with nearly minimum beads are preferred the experimental studies were conducted at 16 kV. Effect of needle length, stand-off distance and voltage on fibre diameter is shown in Fig. 6.
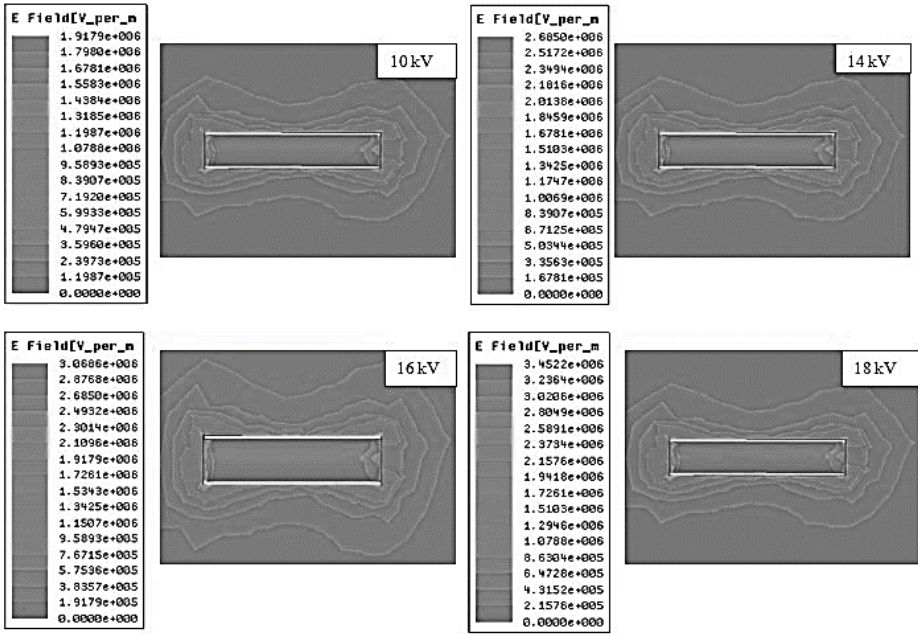
**Fig. 5.** Electric field intensity at varying applied voltage
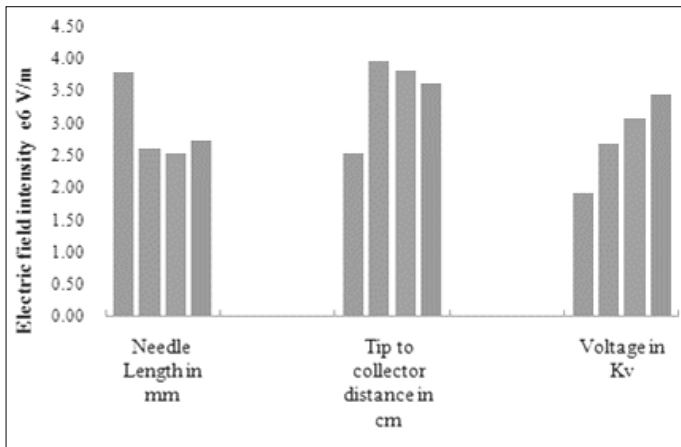


**Fig. 6.** Effect of needle length, stand-off distance and voltage on fibre diameter

## Conclusion

Fibre morphology is an important structural characteristic of electrospun nanofibres. Understanding the impact of processing parameters on morphology of fibres is essential to obtain electrospun nanofibres with desired characteristics. In this work, electrospinning of PCL nanofibres was studied for the influence of applied voltage, solution concentration

and flow rate on fibre diameter and number of beads. Nanofibres of diameter 225±32 nm with nearly no beads were obtained at 10 wt. % of PCL, 16 kV applied voltage and 2 ml / hr flow rate along with thickness, porosity, and mean pore radius of 0.018 mm, 67.76 % and 0.83 µm respectively. SEM micrographs and Image J software were used for fibre diameter and number of beads. Finite element analysis was performed to study relationship of electric field intensity with applied voltage, length of needle and tip to collector distance. Simulation results of maximum electric field intensity corresponded to stand off distance of 15 cm and needle length of 15 mm and applied voltage 18 kV. However, the nanofibres electrospun at this voltage were of large fibre diameters with beads. Finite element simulation guides the parametric optimisation in electrospinning which helps to produce bead free uniform nanofibres

# References

1.   G Sneh, K D Amit, C M Narayan, Fabrication and characterization of PCL/ gelatin composite nanofibrous scaffold for tissue engineering applications by electrospinning method. *Materials Science and Engineering* - 2013, 33, 1228–1235

2.   P T Arjun, K J Mahesh, L Joshua, Heterogeneous electrospun polycaprolactone / polyethylene glycol nanofibres with improved wettability, biocompatibility and mineralization. *Colloids and Surfaces A: Physicochem. Eng. Aspects* - 2017, 520, 105–113

3.   H Mina, B Hajir and Marziyeh Ranjbar-Mohammadi, Fabrication, optimization and characterization of electrospun poly (caprolactone)/gelatine/graphene nanofibrous mats, *Materials Science and Engineering* - 2017, 78, 218–229.

4.   V Narendiran, S Quan, N Joshua, Multifunctional ZnO/Nylon 6 nanofibre mats by an electrospinning–electrospraying hybrid process for use in protective applications. *Science and Technology of Advanced Materials* - 2011, 2, 1-7

5.   L Nina, K J Mahesh, P.T Arjun, Fabrication, characterization and biomedical application of two-nozzle electrospun polycaprolactone / zein-calcium lactate composite nonwoven mat. *Journal of the Mechanical Behaviour of Biomedical Materials* - 2016, 60, 312-323

6.   V Afsaneh, A H  Seyed, Fabrication of Biodegradable PCL Particles as well as PA66 Nanofibres via Air-Sealed Centrifuge Electrospinning (ASCES) „*Journal of Textiles and Polymers* - 2016, 4,15-19

7.  A Sahar, R Azam, Poly (e-caprolactone) electrospun nanofibres containing cinnamon essential oil nanocapsules: A promising technique for controlled release and high solubility, *Journal of Industrial Textiles* - 2018, 48, 1527–1544

8.  A D Maame, Boakye, P R Nava, A Udhab, Fabrication and Characterization of Electrospun PCL-MgO-Keratin-Based Composite Nanofibres for Biomedical Applications, *Materials* - 2015, 8, 4080-4095

9.  G Robabeh , T Giuseppe,  P D Robert , An investigation into the nano-/micro-architecture of electrospun poly-caprolactone and self-assembling peptide fibres. *MRS Advances* - 2016, 1, 711-716

10. B E G Vince, F Y Yining, L Yao, Investigating process-structure relations of ZnO nanofibre via electrospinning method. *Composites* - 2017, 16, 40-45

11. K Shirin, M M Sayed, S Nasser, Hydrophobicity improvement in polyphenylsulfone nanofibrous filtration nanofibres through addition of polyethylene glycol, *Applied Surface Science* - 2015, 359, 252–258

12. D H Reneker, W Kataphinan, A Theron, Nanofibre garlands of polycaprolactone by electrospinning, *Polymer* - 2002, 43, 6785–6794

13. M H Mahabub, A N Khandakar, B H Mohammad, Production of Tissue Engineering Scaffolds from Poly Caprolactone (PCL) and Its Microscopic Analysis, *International Journal of Textile Science* - 2014, 3, 39-43

14. J Artur, Martins, I Ana, A Bourbon, V A António , Physical and mass transfer properties of electrospun polycaprolactone nanofibe, *Process Biochemistry* - 2015, 50, 885–892

15. S Sherif, S Shilpa, W N Jason, Controlling the porosity of fibrous scaffolds by modulating the fibre diameter and packing density. *Journal of Biomedical Materials Research* - 2011, 95, 566-574

16. F D Somayeh, G Farideh , M Bozorgmehr,  Experimental Investigations on Electrospun Mat Production: For Use in High-Performance Air Filters. *International Journal of Occupational Hygiene* - 2015, l, 110-118

17. W Ning, B Krishna, S Wenhui, Tailored fibro-porous structure of electrospun polyurethane nanofibres, their size-dependent properties and trans-nanofibres glucose diffusion. *Journal of Nanofibres Science* - 2013, 27, 207-217

18. W Kang, H Liu, L Li, Simulation of Electric Field Intensity and Electrostatic Force in Electrospinning System Using Finite Element Method, *International Journal of Digital Content Technology and its Applications* - 2013, 7, 750-758

19. W H Duan, J Jiang, Li Bo-Yang, Electric Field Finite Element Analysis and Experimentation of Plate- Plate Type Electrospinning Machine, *International Journal of Control and Automation* - 2014, 7, 179-190

20. S Hadi , M Hamid, H Saeed, Electrospinning of Polyacrylonitrile Nanofibres and Simulation of Electric Field via Finite Element method, *Nanomed Res J* - 2017, 2, 87-92

21. J Jin-gang , H Tian-hua , D Hong-wei,  Electric Field Structure Analysis and Experimentation of Needle-plate Type Electrospinning Machine, *International Journal of Control and Automation* - 2014, 7, 369-378

22. P P Quynh, S Upma and G M Antonios, Electrospinning of Polymeric Nanofibres for Tissue Engineering Applications: A Review. *Tissue engineering* - 2006, 12, 1197-1211

23 N Deogratias, H Wanli ,W Xinhou,  Investigation of a New Needleless Electrospinning Method for the Production of Nanofibres, *Journal of Engineered Fibres and Fabric* - 2013, 8, 42-49

24 C Liu, J Shen, C Z Liao, K W K Yeung, Novel electrospun polyvinylidene fluoride-graphene oxide-silver nanocomposite membranes with protein and bacterial antifouling characteristics. *eXPRESS Polymer Letters* - 2018, 2, 365–382

25. A Ahmed, Ratrouta, J B Martin, B Branko, Wettability in complex porous materials, the mixed-wet state and its relationship to surface roughness, *Proceedings of the National Academy of Sciences of the United States of America* - 2018, 115, 8901–8906

26. H M Bentolhoda, K Shohreh, A K  Haghi,  Surface roughness of electrospun Nanofibrous mats by a novel image processing technique, *Surface Review and Letters* - 2017, 1830005, 1-10

27. H K Hyung, J K Min, J R Su, Effect of Fibre Diameter on Surface Morphology, Mechanical Property and Cell Behavior of Electrospun Poly (ε-caprolactone) Mat, *Fibres and Polymers* - 2016, 17, 1033-1042

28. Z Lingli, S Xingxing, P Xiangfang, Enhanced Hydrophobicity of Electrospun Polyvinylidene Fluoride-Co-Hexafluoropropylene Membranes by Introducing Modified Nanosilic, *Anaheim* - 2017, 586-589

29. T Dan, H H Chun-Hui H Ji-Huan, Macromolecule Orientation in Nanofibres. *Nanomaterials -,* 2018, 8, 1-14